

1 Main Manuscript for

2 Large-scale commodity agriculture exacerbates the climatic impacts of 3 Amazonian deforestation

4 Eduardo Eiji Maeda^{1*}, Temesgen Alemayehu Abera^{1,3}, Mika Siljander¹, Luiz E. O. C. Aragão^{4,5},
5 Yhasmin Mendes de Moura², Janne Heiskanen^{1,3}

6 ¹ Department of Geosciences and Geography, P.O. Box 68, FI-00014 University of Helsinki,
7 Finland

8 ² Royal Society, Newton International Fellow, Centre for Landscape and Climate Research
9 (CLCR), School of Geography Geology and Environment, University of Leicester, UK

10 ³ Institute for Atmospheric and Earth System Research, Faculty of Science, University of Helsinki,
11 Finland

12 ⁴ Remote Sensing Division, National Institute for Space Research (INPE), São José dos Campos,
13 SP, Brazil.

14 ⁵ Geography, College of Life and Environmental Sciences, University of Exeter, Exeter, UK

15

16 * Corresponding author - **email:** eduardo.maeda@helsinki.fi

17

18 Abstract

19 In the Amazon rainforest, land use following deforestation is diverse and dynamic. Mounting
20 evidence indicate that the climatic impacts of forest loss can also vary considerably, depending on
21 specific features of the affected areas. The size of the deforested patches, for instance, was shown
22 to modulate the characteristics of local climatic impacts. Nonetheless, the influence of different
23 types of land use and management strategies on the magnitude of local climatic changes remains
24 uncertain. Here, we evaluated the impacts of large-scale commodity farming and rural settlements
25 on surface temperature, rainfall patterns, and energy fluxes. Our results reveal that changes in
26 land-atmosphere coupling are induced not only by deforestation size, but also by land use type and
27 management patterns inside the deforested areas. We provide evidence that, in comparison with
28 rural settlements, deforestation caused by large-scale commodity agriculture is more likely to
29 reduce convective rainfall and increase land surface temperature. We demonstrate that these
30 differences are mainly caused by a more intensive management of the land, resulting in
31 significantly lower vegetation cover throughout the year, reducing latent heat flux. Our findings
32 indicate an urgent need for alternative agricultural practices, as well as forest restoration, for
33 maintaining ecosystem processes and mitigating change in the local climates across the Amazon
34 basin.

35

36 **Significance Statement**

37 The southern Amazon is one of the fastest changing places on Earth. Deforestation is giving place
38 to a dynamic and diverse landscape, comprising small-scale farmers and large-scale commercial
39 agriculture with differing land uses. Understanding how these different land uses affect ecosystems
40 and local climates is essential for promoting strategies to mitigate environmental changes. Here,
41 we show that large-scale commercial agriculture leads to a higher increase in surface temperature,
42 in comparison with small scale farms. We also found evidence that changes in land surface
43 attributes over large commercial farms lead to a more prominent reduction in rainfall volumes. Our
44 results provide compelling arguments indicating that changes in farming practices are needed to
45 guaranty a sustainable future in the Amazon region.

46

47 **1. Introduction**

48 During the past 50 years, approximately 20% of the Amazon forest has been lost to deforestation
49 (1, 2). These changes in the land surface have affected the functioning of ecosystems and the
50 climate in ways we are only starting to understand. Deforestation size, for instance, is a potential
51 factor defining the magnitude and characteristics of changes in local climate associated with forest
52 loss (3, 4). There is also evidence that the different land uses that follow deforestation can regulate
53 the magnitude of changes in surface energy balance and water cycle (5). Historically, there has
54 been large variation in the characteristics and causes of deforestation (1, 6–9). In the area known
55 as the “arc of deforestation”, two major processes have contributed to forest loss: government
56 supported rural settlements and expansion of market-focused large-scale agriculture (hereinafter
57 referred to as “commodity agriculture”) (10, 11). Deforestation caused by these two types of
58 farming systems have distinct characteristics and each can have several variants.

59 Rural settlements are generally associated with government colonization projects, migratory flow
60 incentives, and the construction of new roads (7). In areas dominated by rural settlements, small
61 properties with plots ranging from 25 ha to 100 ha are predominant (8, 9, 12). However, medium-
62 sized properties ranging from 250 ha to 1000 ha, and farms larger than 1000 ha may also occur.
63 Activities inside these areas are characterized by livestock production (extensive pastures), small
64 scale crop production and family farming (13). The establishment of small farms along main
65 highways and secondary roads results in the well-known “fishbone” deforestation pattern.

66 Forest areas taken by large-scale commodity agriculture represent a more recent stage of
67 occupation, usually associated with spontaneous and economical migration but also to changes in
68 land use policies and market conditions (14). Agricultural activities aimed at commodity crop
69 plantation are in general productive and often technologically advanced. The most common

70 commodity crops in the Amazon region are soybean, maize, sorghum, and cotton. Nonetheless,
71 forests are typically not converted directly into croplands, with pastures often used as a transitory
72 land use. Permanent mid- to large-scale cattle-ranching also occur, although many of these areas
73 are being rapidly converted into croplands (6, 14–16). Farm sizes can reach several thousand
74 hectares. Properties are, therefore, bigger and more isolated, in comparison with rural settlements
75 (13).

76 Given the different characteristics of commodity agriculture and rural settlements, the spatio-
77 temporal patterns of land cover biophysical properties can also differ considerably. In general,
78 commodity crops cultivation involves an intensive use of the land, sometimes with two or more
79 harvests per year (17). Hence, rapid changes in the vegetation cover, albedo, and
80 evapotranspiration can occur (5, 18). On the other hand, in areas where small-scale pastures and
81 agriculture are prevalent, the biophysical properties of the land surface are expected to vary less,
82 given the less intensive use of the land (e.g. associated with family farming and agroforestry).
83 Furthermore, modelling studies suggest that the type of vegetation involved in land cover
84 conversions is important in determining the sign of the land change impacts (19). However,
85 empirical studies are crucially needed to better understand how different land uses across the
86 Amazon region affect the local and regional climate.

87 Tropical deforestation was shown to have deep impacts on environmental processes (1, 20–22), to
88 amplify diurnal temperature variations ($1.95 \pm 0.08^\circ\text{C}$) and increase air temperature ($\sim 1^\circ\text{C}$) (23).
89 The causes of increase in temperature are dominated by non-radiative mechanisms, in particular a
90 decrease in latent heat flux (24). The cooling effects of albedo increase due to deforestation are in
91 most cases outweighed by the warming effects of decreasing evapotranspiration, leading to net
92 warming (23–25).

93 The impacts of Amazon deforestation on rainfall patterns are not yet fully understood (4). In the
94 initial phases of deforestation, vegetation loss was shown to increase regional cloudiness and
95 precipitation (3). In comparison with deforested areas, the greater humidity over forests leads to
96 more convective available potential energy, which makes the atmospheric boundary layer more
97 unstable (26). Conversely, small deforestation patches showed more active shallow convection,
98 explaining the higher frequency of shallow clouds over deforested areas (26). However, it is
99 unclear how these mechanisms change as deforested areas increase and land cover becomes
100 more uniform. One hypothesis is that convective lifting mechanisms will lose force, and shallow
101 clouds over deforested areas will no longer be favored. Modelling studies indicate that this shift is
102 already happening in some parts of the Amazon, where deforestation has reached a point in which
103 thermally dominated regime has declined, leading to a more dynamically driven hydroclimatic
104 regime (27). A dynamically driven regime becomes dominant when differences in surface

105 roughness between forest and forest clearings start to play a larger role in the atmospheric
106 response, in comparison to the differences in the surface energy partitioning (28).

107 As observational and modeling studies indicate that land use and management can play an
108 important role in the climate system, overlooking these landscape heterogeneities can hinder an
109 adequate response to the threats posed by human activities (29). Clarifying the climatic impacts of
110 different land uses in the Amazon is crucial to foster informed plans for sustainable land
111 management, in particular those aiming at strategies for climate change mitigation, maintenance of
112 ecological functioning and guarantying provision of essential ecosystem services. Here, we
113 hypothesize that forest conversion to large-scale commodity agriculture is more detrimental to local
114 climate than conversion to rural settlements. To test this hypothesis, we first evaluated whether or
115 not land uses associated with commodity agriculture and rural settlements lead to quantitatively
116 distinguishable land cover spatio-temporal patterns in regions with similar deforestation rates
117 (1985–2018) and total deforested area in 2018. Next, we collected empirical evidence on how
118 forest clearing associated with these two causes have affected local rainfall, surface temperature,
119 and latent heat flux (LE).

120

121 **2. Results**

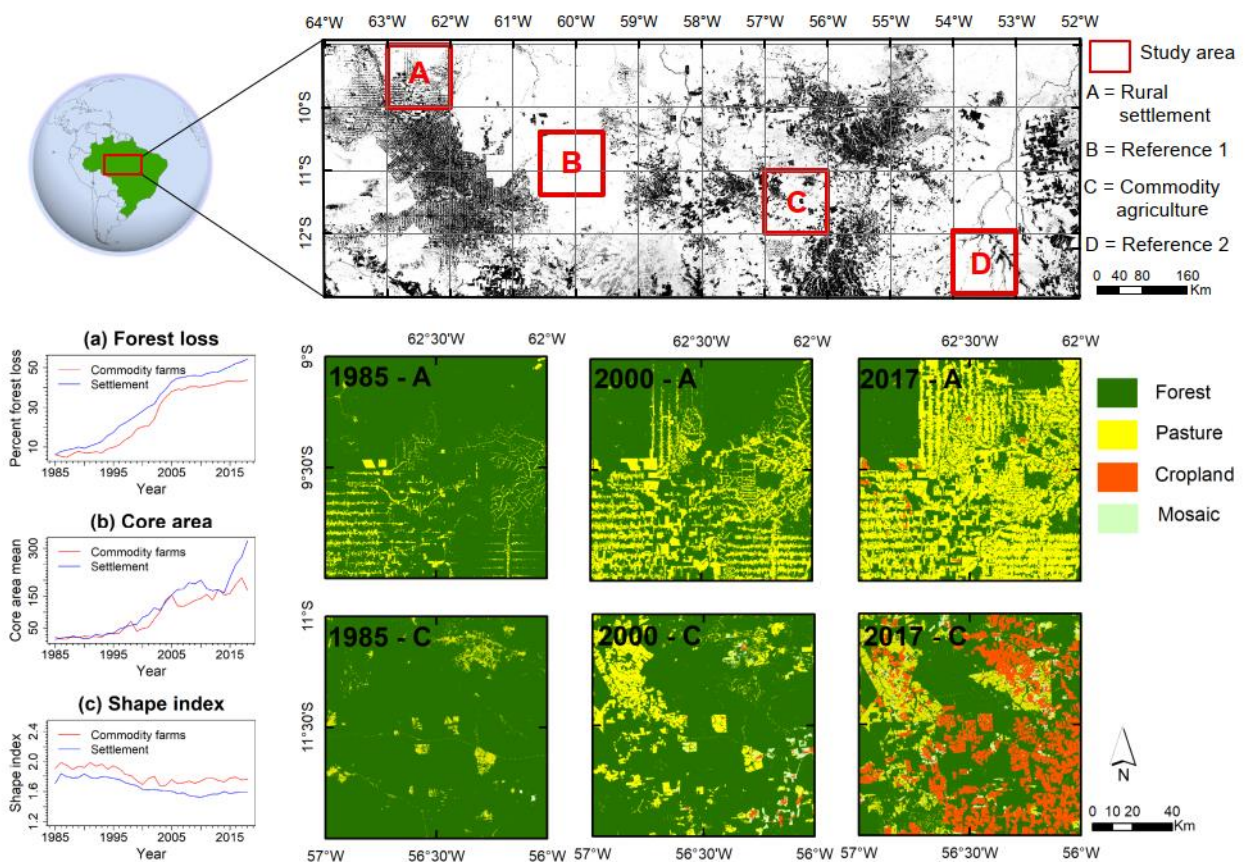
122 **2.1. *Landscape patterns across rural settlements and commodity agriculture*** 123 ***areas***

124 Our analysis focused on four areas (~110 km × 110 km each) in the Amazon basin (Figure 1). The
125 criteria and procedures used to select the study areas are described in section 4.1. Two areas
126 were located in the “arc of deforestation” (marked as A and C in Figure 1). Cell A was located in
127 the State of Rondônia, over an area dominated by a fishbone deforestation pattern, formed by
128 small farms distributed along main highways and secondary roads. Cell C was located in the north
129 of Mato Grosso State, over an area where large-scale commodity farms are prevalent. The mean
130 size of consolidated area per property in Cell A was 52 ha, while in Cell C, the mean size of
131 consolidated area per property was 374 ha (See SI Appendix Fig. S2). In addition, two areas with
132 similar size but not affected by deforestation were used as reference sites (marked as B and D in
133 Figure 1).

134 In both areas affected by land changes (Cells A and C), deforested area in the beginning of the
135 1980's accounted for less than 10% of the total area (Figure 1a). A step increase in forest loss
136 occurred between 1990 and 2005, after which the total area deforested stabilized at approximately
137 40%. Despite similar amount of total area deforested, the spatial patterns of the two regions could
138 be distinguished visually and quantitatively (Figure 1). Until the late 1990's, landscape in both

139 regions displayed similar core area (i.e. the total area of patches that have only neighboring
 140 patches from the same class). After the year 2000, the core area of forests in the area dominated
 141 by fishbone deforestation (“rural settlements”) increased at a higher rate in comparison with areas
 142 allocated for commodity agriculture. The shape complexity, expressed by the shape index (i.e. the
 143 ratio between the perimeter of the patch and the hypothetical minimum perimeter of the patch),
 144 was consistently higher (~10%) in the commodity agriculture areas in comparison to the rural
 145 settlements.

146 Land use in rural settlement areas (Cell A) was largely dominated by pastures throughout the
 147 entire study period, with only small areas designated to croplands (<1%) (Figure 1 and SI
 148 Appendix Fig. S3). Other activities such as family farming and agroforestry, although present, are
 149 likely masked due to the small scale of these activities. Given that these land use types are not
 150 specifically accounted for in the dataset used for this analysis, they are often misclassified as
 151 pastures. In the commodity agriculture area (Cell C), a shift in land use patterns took place after
 152 the year 2000, with a steady increase in areas designated to croplands, reaching approximately
 153 25% of the entire area in 2018. The increase in croplands was accompanied by a decrease in
 154 areas destined to pastures, which decrease from 22%, in 2005, to 13%, in 2018 (Figure 1 and SI
 155 Appendix Fig. S3).



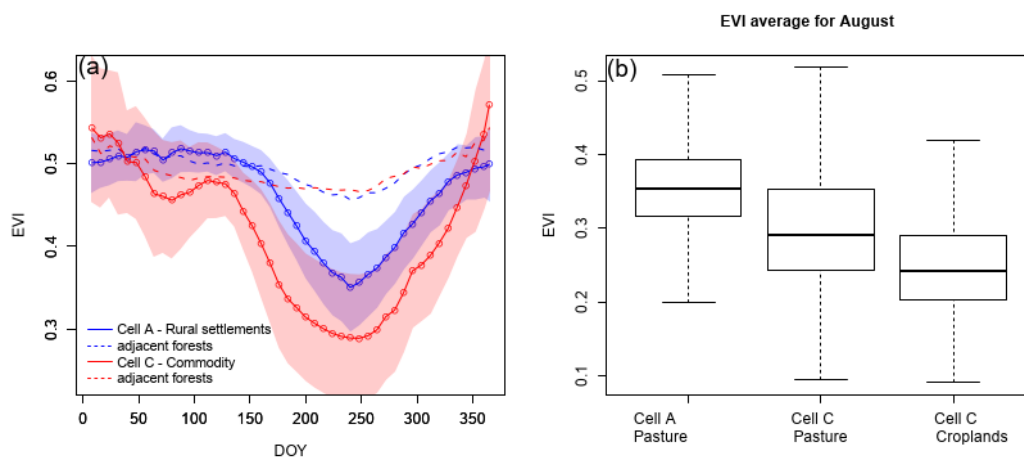
156

157 **Figure 1.** Geographical location of the study areas, each consisting of 1°×1° cells, where: A is
 158 dominated by rural settlements and C large scale commodity agriculture. Cell B and D were used
 159 as reference, as there has been no substantial forest loss in these areas during the study period.

160 (a) Total forest loss, (b) mean core area of deforested areas and (c) the mean shape index of
 161 deforested areas.

162

163 We further demonstrate that land cover temporal patterns differ between the two sites. Vegetation
 164 cover over deforested areas was assessed using satellite derived enhanced vegetation index
 165 (EVI). Areas of commodity agriculture had consistently and significantly (unpaired Welsch t-test,
 166 $p < 0.01$) lower vegetation cover between May (DOY=120) and November (DOY=305) (Figure 2a).
 167 Between December and February, both areas had similar EVI values, indicating a comparable
 168 vegetation cover during this period. We also analyzed differences in the vegetation cover of
 169 dominant land use types in our study areas. In September, when vegetation cover was shown to
 170 be the lowest, croplands had approximately 20% lower EVI than pastures inside the same region
 171 (i.e. Cell C, mid- to large-scale cattle-ranching), and 30% lower than pastures located in the rural
 172 settlement area (Cell A).



173

174 **Figure 2.** (a) Seasonal variability in vegetation cover inside deforested areas (solid lines) and in
 175 adjacent forests (dashed lines) measured using the Enhanced Vegetation Index (EVI). The
 176 adjacent forests represent intact forests located inside the same 1°×1° cell. Average values
 177 calculated using data from 2001–2018. DOY=Day of Year. Shaded areas represent mean ±
 178 standard deviation. (b) August average EVI values for dominant land use classes inside each cell.

179

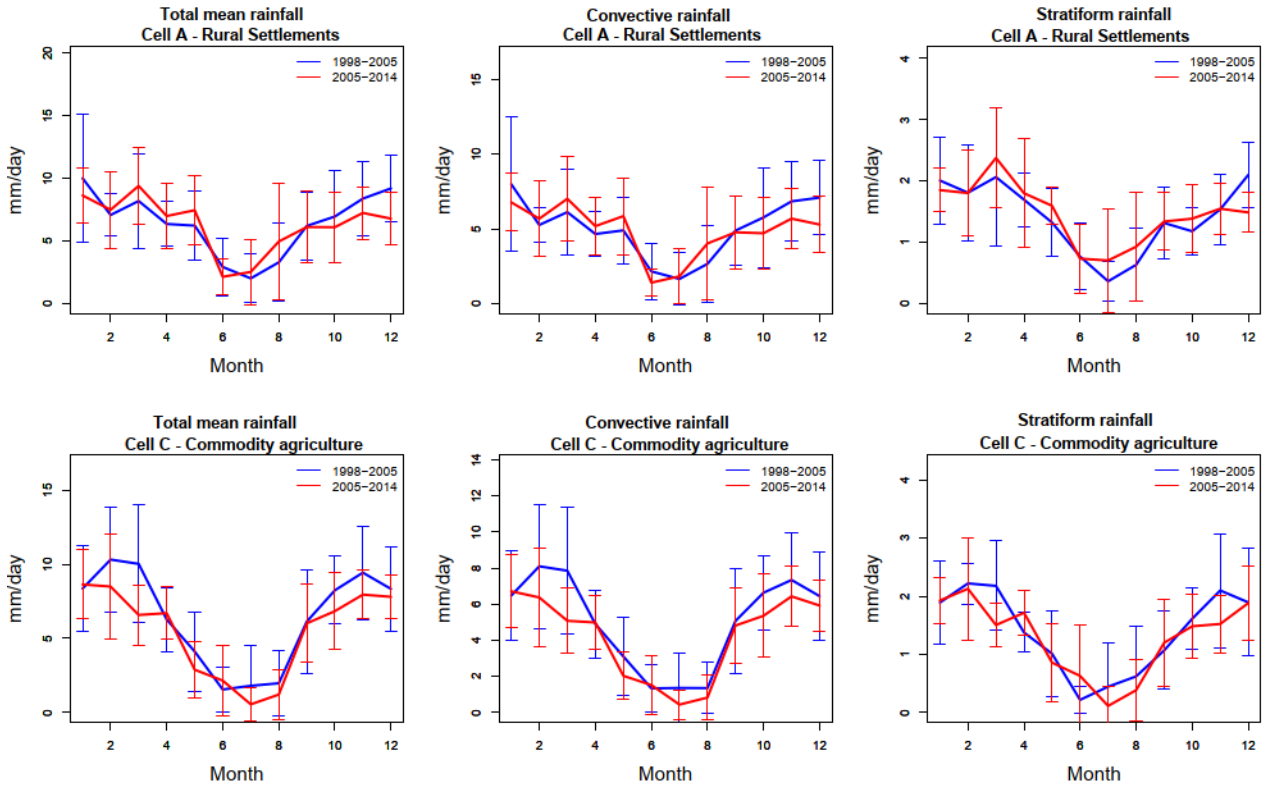
180 **2.2. Changes in rainfall patterns**

181 Changes in the seasonal patterns of rainfall were evaluated based on the average of two periods:
182 from 1998 to 2005, and from 2005 to 2014 (Figure 3), thus comprising the entire time-series of the
183 TRMM (Tropical Rainfall Measuring Mission) precipitation radar. These time intervals allowed the
184 assessment of rainfall patterns from a period when deforestation process was only beginning, to a
185 period when forest loss was relatively stable. The average forest cover percentage in Cells A and
186 C, was at 83% from 1998 to 2005, and declined to 57% from 2005 to 2014.

187 We observed decreasing rainfall rates in the commodity agriculture site (Figure 3 and Figure 4).
188 The reduction occurred mostly during months with average monthly rainfall above 200 mm month⁻¹
189 (i.e. the period between October and March, hereinafter referred to as “wet season”), being
190 particularly evident in February, March, October and November. The decrease was shown to be
191 mainly caused by a reduction in convective rainfall, while changes in stratiform rain were less
192 evident (Figure 3). When considering the annual mean, we observed significant differences in the
193 mean total and convective rain ($p=0.016$ and 0.009 , respectively, based on a Welsch t-test), while
194 differences in the mean annual stratiform rain were not significant ($p=0.279$). A Mann-Kendall (M-
195 K) trend test indicated a strong and consistent decreasing trend in convective rainfall ($p=0.006$)
196 during the wet season between 1998 and 2014, while the stratiform rainfall trend during the same
197 period had a lower magnitude ($p=0.012$) (Figure 4). There were no significant trends in rainfall
198 during the dry season (Apr–Sep) in the commodity agriculture site (Figure 4).

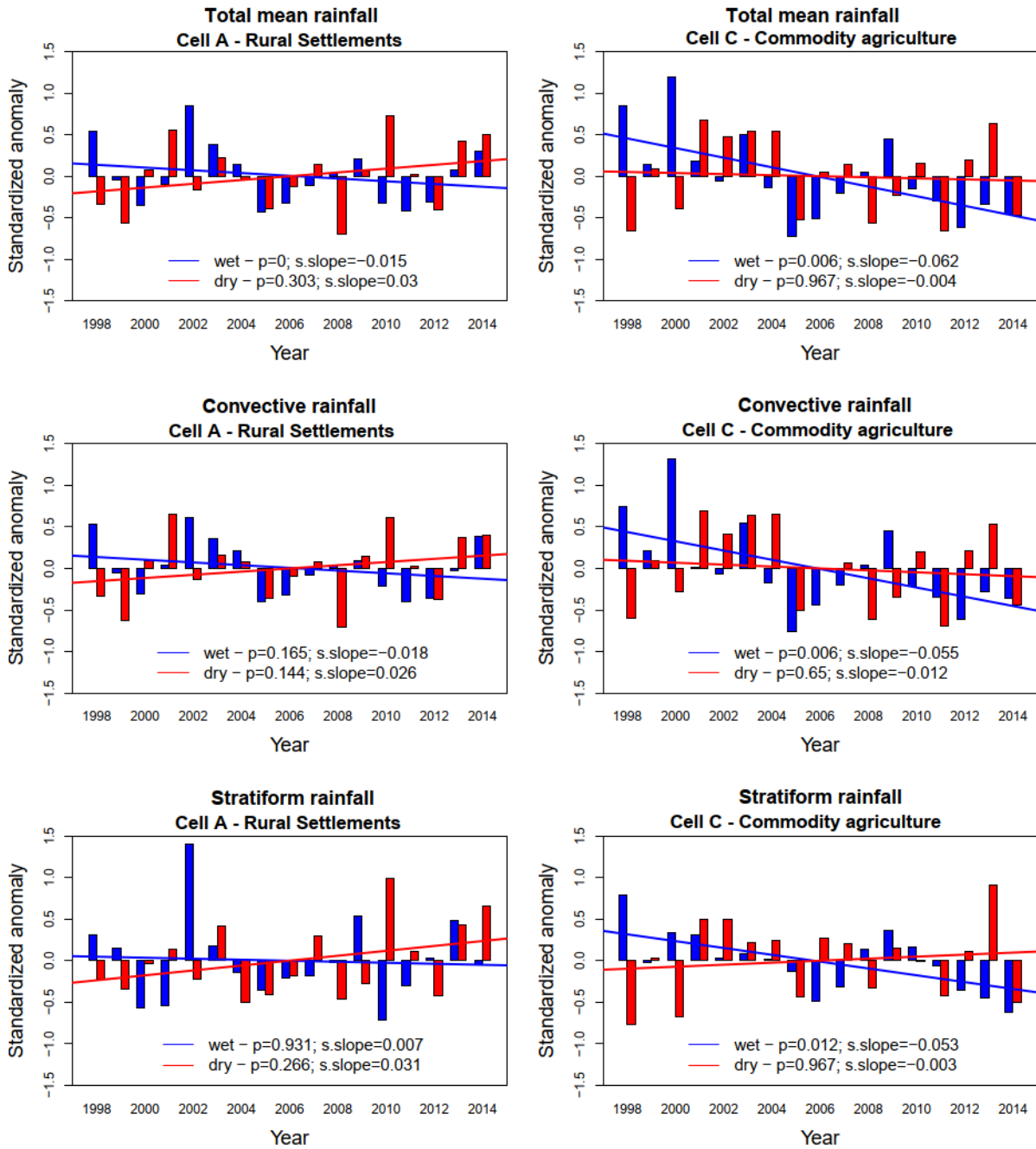
199 In the rural settlements site, there were no clear changes in the seasonal patterns of rainfall
200 between the two periods (Figure 3). Annual mean values were also not statistically different (based
201 on a paired Welsch t-test). This result was confirmed by the M-K test, which did not indicate
202 significant trends in convective or stratiform rainfall, independently of the season (Figure 4).

203 To discard the influence of large-scale climatic signals in these results, we conducted the same
204 analysis in two reference areas (i.e. Cell B, located between cells A and C in the northwest part of
205 Mato Grosso State, and Cell D, located inside the Xingu National Park - both areas showed no
206 forest loss during the same period of time) (Figure 1; Supplementary figures S1, S4 and S5). The
207 results confirmed that significant trends were not observed in the regions unaffected by
208 deforestation.



209

210 **Figure 3.** Mean seasonal patterns of rainfall between 1998–2005 (blue lines – average forest
 211 cover = 83%) and 2005-2014 (red lines – average forest cover = 57%).



212

213 **Figure 4.** Rainfall time-series trends from 1998 to 2014. The wet period (blue) is represented by
 214 average rainfall values from October to March, while the dry period (red) is represented by the
 215 period between April and September. We define wet period as the period when average monthly
 216 rainfall in our study areas were above 200 mm month⁻¹.

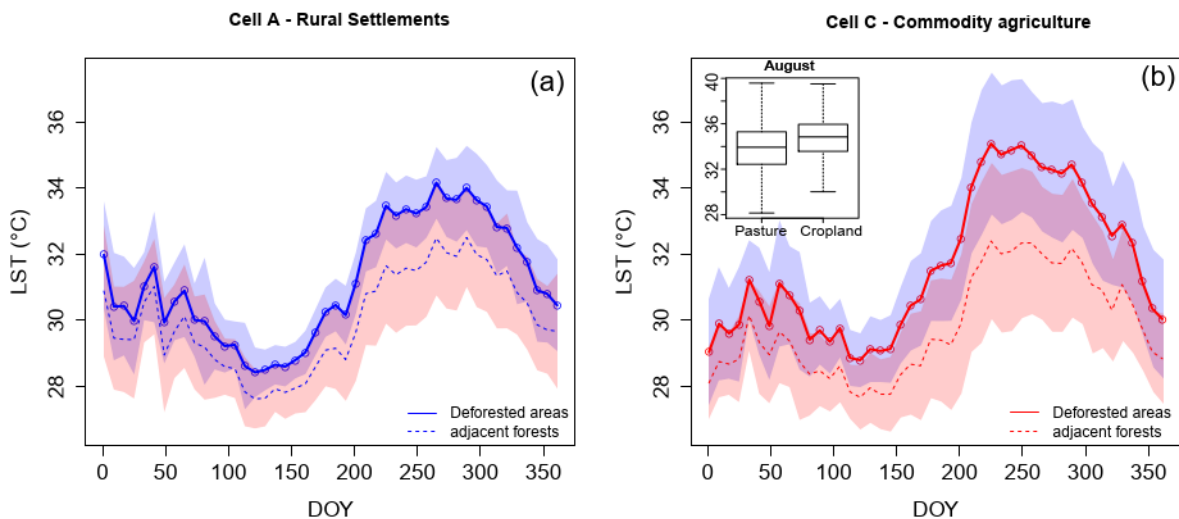
217

218 **2.3. Changes in land surface temperature and latent heat flux**

219 Changes in land surface temperature (LST), latent heat flux (LE) and evapotranspiration (ET)
 220 caused by forest loss were assessed using a space-for-time substitution approach (30, 31). The

221 basic assumption in the space-for-time substitution is that spatial and temporal variation are
 222 equivalent (30). Hence, observations over deforested areas were compared with those obtained
 223 over adjacent forests. We observed that both sites showed significant differences in LST between
 224 forested and deforested areas ($p < 0.01$) (Figure 5). These changes were present during all seasons
 225 of the year, although differences in the dry season had higher magnitude. Forest loss associated
 226 with rural settlements caused an average LST increase of 1.05 °C during the wet seasons and
 227 1.25 °C during the dry seasons (Figure 5a). The maximum average warming in rural settlement
 228 areas was observed in August (1.85 °C). In areas of commodity agriculture, warmings of 1.57 °C
 229 and 2.11 °C were observed in the wet and dry seasons, respectively. The maximum difference was
 230 also observed in August (3.06 °C). When untangling these results by land use type, we observed
 231 that, in August, croplands were on average approximately 1 °C warmer than pastures (Figure 5).
 232 Both pastures in Cell A and Cell C showed similar mean temperature for the same period (33.8 °C
 233 and 33.2 °C, respectively).

234



235

236 **Figure 5.** Mean seasonal patterns of land surface temperature in (a) rural settlements and (b)
 237 commodity agriculture areas, with boxplots showing results for dominant land use classes within
 238 the region. Average values calculated using data from 2001–2018. Shaded areas represent mean
 239 \pm standard deviation.

240

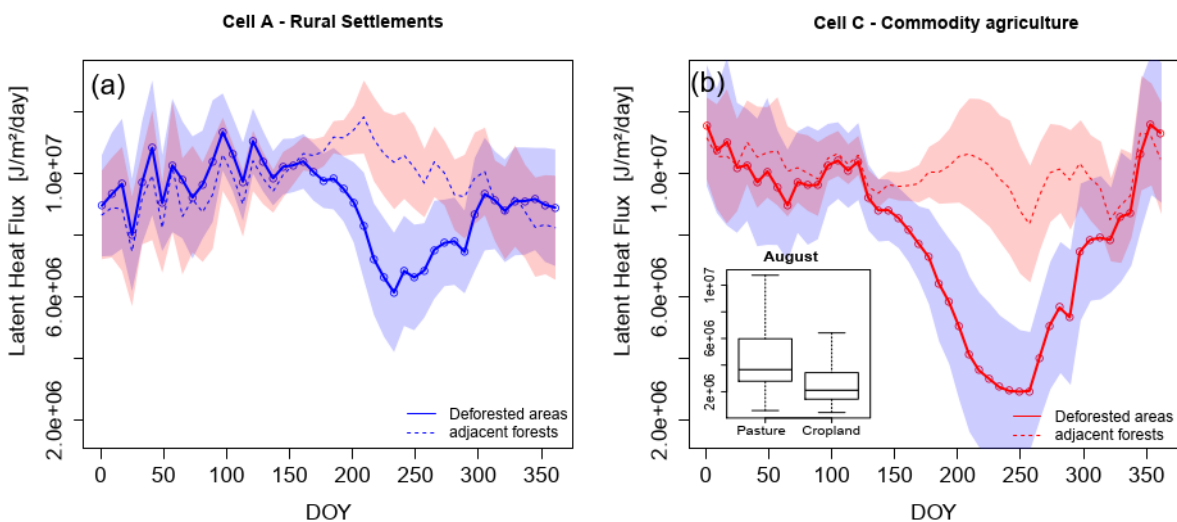
241 Changes in LE caused by forest loss were evident in both sites (Figure 6). The magnitude and
 242 seasonal patterns of the changes were, however, more pronounced in deforested areas caused by
 243 commodity agriculture. In rural settlement areas, the decline of LE (in relation to adjacent forests)
 244 was observed from June (DOY≈150) to the end of October (DOY≈300). In commodity agriculture

245 areas, the decline occurred from May (DOY≈125) to mid-November (DOY≈325) i.e. approximately
 246 50 days longer than the rural settlements area. In both areas, the strongest reduction in LE was
 247 observed around August–September. During this period, the LE decline in commodity agriculture
 248 areas was approximately two times larger than in fishbone areas (Figure 6). During August,
 249 croplands had 39% lower LE than pastures located in the same region (Cell C) and 60% lower LE
 250 than pastures located in rural settlement areas (Cell A).

251 Changes in ET followed the same pattern (SI Appendix Fig. S7a). In commodity agriculture areas,
 252 the lowest ET values were around 1.2 mm day^{-1} (compared to $3\text{--}4 \text{ mm day}^{-1}$ in adjacent forests),
 253 while the minimum ET in fishbone areas reached $\sim 2.4 \text{ mm day}^{-1}$. The contribution of transpiration
 254 to total ET ($T/(E + T)$) was consistently lower in commodity agriculture areas, in comparison with
 255 rural settlements (Figures S7b, S7c, S7d), confirming the key role of vegetation cover on the
 256 stronger reduction of LE and ET in commodity agriculture areas. During August–September, when
 257 the strongest reduction in LE was observed, $T/(E+T)$ was approximately 60% in commodity
 258 agriculture areas, and 75% in rural settlements (Figures S7b).

259 Contrasting differences were also observed in the rainy season, particularly from January to May
 260 (Figure 6 and S7). During this period, rural settlement areas showed similar or higher LE and ET in
 261 comparison to adjacent forest areas. On the other hand, in commodity agriculture areas, LE and
 262 ET values were lower than in the original land cover, in particular between February and April (i.e.
 263 same period when a reduction in convective rainfall was observed). This result is again explained
 264 by a lower contribution of T to total ET, which was as low as 75% between January and May in
 265 commodity agriculture areas (in comparison to 80% in rural settlements) (Figures S7b).

266



267

268 **Figure 6.** Mean seasonal patterns of latent heat flux in (a) rural settlements and (b) commodity
269 agriculture areas, with boxplots showing results for dominant land use classes within the region.
270 Average values calculated using data from 2001–2018. Shaded areas represent mean \pm standard
271 deviation.

272

273 **3. Discussion**

274 Our results demonstrate that taking into account the complex combination of matrix shape, land
275 use, and land management is key to understanding the climate impacts caused by deforestation in
276 the Amazon forest. We provided evidence that regions with similar history of total forest loss can
277 have quantitatively distinguishable spatial patterns, depending on the original causes of
278 deforestation, leading to different climate impacts.

279 We report a significant decline in wet season rainfall volumes in areas dominated by large scale
280 commodity agriculture. The same decline was not observed in an area where deforestation was
281 mainly caused by rural settlements. Although the observed association between these two
282 deforestation types and rainfall changes cannot prove a causal link, evidence from the causality
283 can be deduced from the underlying physics driving the rainfall formation process. Previously
284 published research collected evidence that changes in land-surface properties can influence
285 energy and moisture fluxes within the planetary boundary layer, as well as convective available
286 potential energy, strongly affecting the development of cumulus convective rainfall (32). Modelling
287 studies demonstrated that, as deforested areas increase and land cover becomes more uniform,
288 convective lifting mechanisms lose force and local surface roughness start to play a larger role in
289 the regional climate dynamics (27). The decreasing rainfall in commodity agriculture areas could
290 then be explained by the stronger reduction in LE in comparison with rural settlements, which leads
291 to increasing aridity and weakening of convective lifting (33). This argument is confirmed by a
292 stronger vapor pressure deficit (VPD) increase in the region dominated by commodity agriculture,
293 in comparison with the rural settlement area (See SI Appendix Fig. S8). Within the commodity
294 agriculture area, VPD in croplands was on average 5% higher than in pastures (and 10% higher
295 than in pastures located in the rural settlement region).

296 Although the decrease in ET had a higher magnitude during the dry season, the effects of reduced
297 ET on convective rainfall seemed more evident at the end of the rainy season (February–April).
298 These findings are in line with previous studies indicating that ET reduction and surface warming
299 lead to the drying of the atmospheric boundary layer, hindering cloud formation and reducing
300 rainfall (34). Studies have also demonstrated a large influence of forest loss on the ET patterns in
301 the Southern Amazon, reinforcing the role of forests in recycling precipitation by returning soil
302 moisture back into the atmosphere (35).

303 The lower LE in commodity agriculture areas are likely explained by land management and crop
304 phenology. Given the long growing season in Southern Amazon, crop production cycles are more
305 complex than traditional cropping cycles found in temperate regions. In Mato Grosso State, for
306 instance, the agricultural calendar can consist of multiple harvesting and seeding seasons (36).
307 Soybean and maize seeding usually takes place between September and November, and
308 harvesting between January and May. This can be followed by another crop growing season
309 (referred as “safrinha” in Portuguese), which occurs between February and September, usually
310 consisting of maize or cotton.

311 The harvesting and seeding cycles typical for commodity crops lead to abrupt changes in the land
312 surface properties, given the reduction of vegetation cover and exposure of bare land (18, 37, 38).
313 This pattern is confirmed by the analysis of the EVI patterns over our sites. EVI is strongly related
314 to photosynthetically active vegetation biomass (39, 40), and was shown to be efficient in
315 monitoring agricultural production cycles (17), being a good indicator for crop mapping in Southern
316 Amazon (36). All these combined, contribute for lower plant transpiration, reduced soil moisture,
317 and changes in the surface energy balance. Such abrupt changes in the land surface are less
318 likely to occur in rural settlement areas, given the different land use dynamics in these regions.
319 Rural settlements are mostly characterized by pastures. Family farming and agroforestry also
320 occur at smaller scales, which result in a more stable vegetation cover of the land surface, as the
321 soil is not tilled or exposed during harvest.

322 When deforestation occurs, several factors contribute to changing the energy balance, which may
323 lead either to the cooling or warming of the land surface. The resulting effects are mainly driven by
324 two competing biophysical factors, ET and albedo (41). Forests appear darker than shorter
325 vegetation (42, 43); consequently, forest loss often increase surface albedo (i.e. lower absorption
326 of shortwave radiation), contributing for surface cooling. However, in tropical regions, non-radiative
327 mechanisms (i.e. ET, surface roughness) are by far the dominant processes in energy budget
328 changes caused by deforestation, leading to net warming (19, 24, 25, 41). Our results further refine
329 these findings, demonstrating that land use and management patterns following deforestation are
330 also critical for defining spatio-temporal patterns of surface energy balance. Overall, this is in line
331 with previous studies indicating that forest-to-crop transitions have a more detrimental effect on ET,
332 LE and net surface radiation, when compared to forest-to-pasture transitions (5, 19).

333 However, the impacts of large-scale oscillations on the local climate trends observed in our study
334 cannot be discarded, particularly the influence of atmospheric circulation patterns on the rainfall
335 changes. Likewise, disentangling the effects of climate variability and land cover change on
336 regional rainfall is challenging, as climate effects can mask deforestation-induced changes to the
337 water budget (44). To improve our understanding of the ongoing climate changes in our study

338 areas, we analyzed a time series of mean vertically integrated moisture divergence, which
339 represents the horizontal rate of moisture flow (SI Appendix Fig. S9). This parameter is positive for
340 moisture that is spreading out, and negative for the opposite, for moisture that is concentrating.
341 Therefore, it indicates whether atmospheric motions act to decrease (for divergence) or increase
342 (for convergence) the vertical integral of moisture, over the time period. Interestingly, our results
343 indicate a decreasing trend of moisture divergence (increasing convergence) during the wet
344 season, over all our study sites (SI Appendix Fig. S9). These results are in line with previous
345 research indicating that the Amazon basin has become substantially wetter since the 1990's,
346 mainly due to increasing atmospheric water vapor import from the warming tropical Atlantic (45).
347 This trend coincides with the onset of an increasing trend in tropical Atlantic sea surface
348 temperatures (45). Thus, given the increasing moisture convergence in all study areas, our results
349 provide evidence that the decreasing precipitation trend observed in commodity agriculture areas
350 can be caused by local changes in land surface biophysical attributes.

351 The spatial (fishbone) patterns of deforestation caused by rural settlements have been known for
352 decades. The higher shape index and core area of rural settlements demonstrate a greater overall
353 landscape complexity in areas of rural settlement (46). The higher core area in rural settlements
354 are initially counter intuitive, given that the region is characterized by smaller rural properties. The
355 core area is defined as all cells that have no neighbor with a different class than themselves.
356 Hence, our result in the rural settlement area is explained by a stronger connectivity between
357 patches, which results in larger core areas, even though these areas may comprise several
358 different rural properties.

359 Previous studies have gathered compelling evidence that the size of deforested areas is also
360 important in defining the characteristics of local climatic changes. Small scale forest loss was
361 shown to increase regional cloudiness and precipitation frequency, due to enhanced mass and
362 energy transfers between the land and the atmosphere (3, 26). On the other hand, this thermally
363 triggered atmospheric circulation tends to get weaker as deforested areas size increases, reducing
364 rainfall rates (4, 27). Our results demonstrate that changes in land-atmosphere coupling are
365 defined not only by the size of deforested areas, but are strongly dependent on land use and
366 management patterns inside those areas.

367 These findings reinforce the argument that the impacts of modification and management of the
368 land merit the same level of research and policy attention given to other anthropogenic
369 contributions to climate change (47). We suggest that practices aiming to maximize vegetation
370 cover should be further explored to mitigate changes in climate. These include, for instance,
371 agroforestry or perennial crops cultivation (48). Agroforestry is a particularly attractive option, as it
372 seeks to manage forest services and agriculture at the same time, improving soil fertility,

373 increasing water availability, while preserving vegetation cover and microclimate. Agroforestry
374 systems are currently a very small element of the agricultural landscape in the Amazon, often at
375 experimental scales or as a result of internationally funded initiatives (49).

376 Integrated crop-livestock systems are seen as a potential pathway to increase low productivity and
377 sustainability of cattle production in the Amazon. The integrated soybean-cattle systems can have
378 higher productivity than continuously grazed areas, and hence, increased resilience under
379 changing climate (50). In suitable areas, integrated crop-livestock systems can be also very
380 profitable (51). However, both intercropping and rotation systems decrease vegetation cover in
381 comparison to cattle grazing systems. Therefore, systems that include also trees (integrated
382 crop-livestock-forestry systems) are recommended, considering our results.

383 On the other hand, traditional commodity agriculture in the Southern Amazon is very productive,
384 profitable and technologically advanced. It is therefore farfetched to assume that alternative
385 methods will replace the current system in a short-term and at large scales. However, with
386 increasing international awareness and consumers' preference for more sustainable products,
387 alternative production methods will start to become more attractive. Actions led by the food
388 industry and civil society organizations have been proven useful to guide in the direction of more
389 sustainable practices. For instance, Brazil's soy moratorium, signed in 2006 by major soybean
390 traders, limited the commercialization of soy grown on lands deforested after July 2006 in the
391 Brazilian Amazon, having a positive impact on the reduction of deforestation rates, while not
392 affecting agricultural production (52, 53). Furthermore, there is increasing evidence that public
393 policies, in combination with international trade treaties and protocols, have positive effects on
394 sustainable land use and thus the climate system (29).

395 Finally, restoration of legal forest reserves is another important pathway to mitigate changes in the
396 regional climate. The recently created Rural Environmental Registry of private properties (CAR) will
397 provide an unprecedented tool to monitor the compliance with the Brazilian forest code, by linking
398 a responsible land-holder to land use on a particular farm (52, 53). This will thus allow the
399 identification of suitable areas for forest restoration, as well as the creation of more sustainable
400 supply chains.

401

402 **4. Material and methods**

403 **4.1. Study areas**

404 We selected four areas of ~110 km x 110 km each (1° x 1°) (Figure 1). As our aim was to compare
405 areas dominated by commodity agriculture and rural settlements, we carried a search for regions

406 having similar total deforested area throughout the study period, but distinct land use and spatial
407 patterns. To select the suitable regions, the study areas had to meet the following criteria:

- 408 ▪ Have similar total deforested area
- 409 ▪ Have similar temporal rates of deforestation within the analyzed time-window
- 410 ▪ Be big enough to provide a representative sampling, and contain enough pixels from the
411 remotely sensed data that were being evaluated (e.g. TRMM data at 0.25 degrees)
- 412 ▪ Be small enough to avoid confounding factors such as climate variability due to latitudinal
413 differences or regional variability
- 414 ▪ Have very distinct land use pattern i.e. one needed to be dominated by rural settlements,
415 and the other need to be dominated by large-scale commodity agriculture
- 416 ▪ Be far away apart to avoid spatial-autocorrelation of rainfall data.

417 To identify the regions meeting all the above criteria, we first divided the entire Amazon basin in a
418 1° x 1° grid. This cell size (i.e. ~110 km x 110 km) was considered consistent with the spatial
419 resolution of all remote sensing datasets used in the study. The total deforested areas inside each
420 cell was calculated using land cover maps from MapBiomass project (<https://mapbiomas.org/en>)
421 (see section 4.2 for details). After identifying cells with similar total deforestation trajectories, we
422 selected regions with distinct land use patterns based on: a) visual interpretation of spatial
423 deforestation patterns; b) size of rural properties according to the CAR and c) predominance of
424 commodity crops, as identified in by land use maps from MapBiomass project. The CAR is a
425 mandatory and self-declaratory electronic registry for rural properties, in which owners must
426 provide georeferenced data on the boundaries of the properties, as well as other information such
427 as legal reserve areas, and areas deforested.

428 We were also careful to select cells that were far away apart to avoid spatial-autocorrelation in the
429 analysis of rainfall data. Rainfall patterns are defined not only by local land surface properties, but
430 also by boundary conditions (e.g. synoptic conditions, atmospheric circulation). A study using more
431 than 800 meteorological stations, showed that the correlation coefficients of rainfall occurrence
432 measured by stations distanced by less than 100 km were mostly above 0.8, decreasing to 0.4 or
433 less, for stations distanced by more than 500 km (54). The selected commodity agriculture and
434 rural settlement regions are approximately 550 km apart, thus avoiding major issues with spatial-
435 autocorrelation.

436

437 **4.2. Land use and land cover data**

438 Land use and land cover data were obtained from the MapBiomas project¹. We used the Collection
439 4, released in August 2019, covering the period from 1985 to 2018. This product offers land use
440 and land cover maps at a 30 m spatial resolution. The maps are produced annually, based on the
441 classification of Landsat imagery mosaics. The mosaics are formed by a composition of the best
442 quality pixels in each set of images for a certain time period. The mosaics are then used to
443 produce a map with land cover classes (forest, agriculture, pasture, urban area, water, etc.) using
444 random forest algorithm. All data are public and free for non-commercial use or general interest
445 purposes. In this study, we re-classified the maps into four classes: forest, pasture, cropland, and
446 mixed-use. These four classes accounted for more than 99% of the total area in our study sites,
447 during the entire study period. The forest class aggregated all the natural vegetation areas that did
448 not suffer any conversion during the study period.

449

450 **4.3. Landscape metrics**

451 To describe landscape patterns in the study areas affected by deforestation (marked as A and C in
452 Figure 1), we calculated landscape metrics for forest and non-forest land cover classes using
453 FRAGSTATS 4.2 (46). Due to redundancy of the information provided by the various landscape
454 metrics, we used Pearson correlation test to discard highly correlated metrics ($r \geq 0.80$). From the
455 remaining eight metrics, we selected two that were less correlated with total forest loss (i.e. were
456 more sensitive to landscape patterns/complexity and less sensitive to the class total area): mean
457 shape index and mean core area (55). The shape index is the ratio between the perimeter of the
458 patch and the hypothetical minimum perimeter of the patch. It equals zero if all patches have an
459 identical shape index and increases, without limit, as the shapes of patches become more
460 complex. The core area is defined by the cells that have only neighbouring cells from the same
461 class, and the mean core area equals the mean of core areas of all patches belonging to a certain
462 class (46).

463

464 **4.4. Enhanced vegetation index (EVI)**

465 Vegetation cover over deforested areas was assessed using satellite derived enhanced vegetation
466 index (EVI), which is calculated based on the reflectance (ρ) of red, blue and near-infrared (NIR)
467 (40) following equation 1:

¹ "MapBiomas Project - Collection 4 of the Annual Land Use Land Cover Maps of Brazil, accessed through the link: <https://mapbiomas.org>". MapBiomas Project is a multi-institutional initiative to generate annual land use land cover maps based on automatic classification processes applied to satellite images. The complete project description can be found at <http://mapbiomas.org>"

$$468 \quad EVI = G \times \frac{(\rho_{NIR} - \rho_{Red})}{(\rho_{NIR} + C1 \times \rho_{Red} - C2 \times \rho_{Blue} + L)} \quad (1)$$

469 where ρ_{NIR} is the near infrared reflectance factor, ρ_{Red} is the red reflectance factor, ρ_{Blue} is the blue
 470 reflectance factor, and the coefficients adopted were: $L=1$, $C1 = 6$, $C2 = 7.5$, and $G= 2.5$.

471 The imagery were obtained from the MODIS Multi-Angle Implementation of Atmospheric
 472 Correction (MAIAC) product (MCD19A1) (56), at 1 km spatial resolution, which was downloaded
 473 from NASA's Level 1 and Atmosphere Archive and Distribution System (LAADS). We used MODIS
 474 Collection 6 Level 1B (calibrated and geometrically corrected) observations, which removed major
 475 sensor calibration degradation effects present in earlier collections. Observations collected
 476 between 2001 and 2018 were used in this study. MAIAC uses an adaptive time series analysis and
 477 processing of groups of pixels for advanced cloud detection, aerosol retrieval and atmospheric
 478 correction. The data are corrected for sun-sensor-target geometry effects inherent of the image
 479 acquisition process. All the images are normalized to an apparent nadir view zenith angle (0°) and
 480 45° of solar zenith angle using a bidirectional reflectance distribution function (BRDF) and Ross-
 481 Thick Li-Sparse (RTLS) model (56).

482 **4.5. Rainfall data**

483 Rainfall data were obtained from the Tropical Rainfall Measuring Mission (TRMM) satellite, which
 484 was launched in November 1997 (57), and shut down in 2015. The product used was the 3A25,
 485 which consists of monthly statistics of the precipitation radar (PR) measurements (58). We used
 486 the $0.5^\circ \times 0.5^\circ$ resolution grid, with monthly mean values of surface rainfall rate, which are
 487 classified between stratiform and convective types. The rain type classification in TRMM PR
 488 products is done using two methods: the vertical profile method (59) and the horizontal pattern
 489 method (60). The vertical profile method is largely based on the detection of the bright band (BB),
 490 which indicates a melting layer, where the solid particles melt and change into rain drops. In the
 491 case of stratiform rain, the BB appears as a strong signal of radar echo when the radar frequency
 492 is between 15 to 20 GHz (59). This dataset and other TRMM data can be obtained through NASA's
 493 EARTHDATA search portal (<https://search.earthdata.nasa.gov/search>).

494 **4.6. Land surface temperature**

495 Land surface temperature (LST) data were obtained from the Moderate Resolution Imaging
 496 Spectroradiometer (MODIS). The product used was the MOD11C2 Version 6, which provides LST
 497 imagery in a $0.05^\circ \times 0.05^\circ$ latitude/longitude grid. The LST values in the MOD11C2 imagery are
 498 provided as composites, with pixel values representing the average of clear-sky LST during an 8-
 499 day period (61). All 8-day composites from 2001 to 2018 were used in this study.

500 The LST represents the radiometric temperature related to the thermal infrared radiation emitted
501 from the land surface observed by an instantaneous MODIS observation. In this study, we used
502 the daytime LST, corresponding to measurements obtained around 10:30 a.m. (local solar time).
503 The MODIS LST products have been validated over a broad range of representative conditions
504 and extensively tested using comparisons with in-situ values and radiance-based validation. The
505 product uncertainties are well defined, with LST errors estimated to be lower than 1 K in most
506 cases (62).

507 In land areas, MODIS LST is only calculated for pixels at clear-sky conditions at 95% confidence
508 for regions below 2000 m a.s.l. and 66% confidence for regions above 2000 m a.s.l. (61). In our
509 study, a quality control was undertaken using the quality assurance (QA) layers provided with the
510 MOD11C2 product. The QA layer was used to exclude pixels in which LST was not produced due
511 to atmospheric interference or not processed due to poor quality. Pixels with average LST error
512 higher than 1 K were also excluded.

513 LST is known to be strongly affected by land cover characteristics (63–65). Given the different
514 spatial resolutions between the LST data and the land cover maps, we carried out an additional
515 analysis using high resolution LST to exclude the influence of pixel mixture on our results. For that,
516 we used a Landsat 8 based LST product with 30 m spatial resolution (66) (SI Appendix Fig. S6).
517 This product was shown to have an overall RMSE of 1.52 °C, based on a comparison against two
518 independently produced reference datasets. All cloud free scenes obtained in dry seasons from
519 2013 to 2018 were considered, resulting in the five suitable images. The results obtained using the
520 30 m Landsat 8 LST product concurred with the conclusions based on the MODIS data, showing
521 that areas occupied by commodity agriculture present significantly higher LST in comparison with
522 areas occupied by rural settlements (SI Appendix Fig. S6).

523 **4.7. Vapor pressure deficit (VPD)**

524 Vapor pressure deficit (VPD) was assessed using a remote sensing approach proposed by
525 Hashimoto et al (2008) (67). This method uses linear models to predict VPD using saturated vapor
526 pressure calculated from MODIS LST. The saturation vapor pressure was calculated as follow
527 (67):

$$528 \quad e^*(T) = 0.6107e^{(17.38T)/(239+T)} \quad (2)$$

529 where $e^*(T)$ is given in kPa and T is the LST estimated by the MODIS sensor at around 10:30 a.m.
530 VPD was then calculated using the following linear model (67):

$$531 \quad VPD = 0.353e^*(T) + 0.154 \quad (3)$$

532 Hashimoto et al (2008) (67) tested this model in Porto Velho, in the Brazilian Amazon, reporting a
533 root-mean-squared-error (RMSE) of 0.35 and a mean absolute error (MAE) of 0.27.

534

535 **4.8. Latent heat flux, Evaporation and Transpiration**

536 Latent heat flux (LE) and Evapotranspiration (ET) 8-day composite data, produced at 500 m spatial
537 resolution, were obtained from the MODIS MOD16A2 product (68). LE is an important component
538 of Earth's surface energy budget. It describes flux of energy from the land surface to the
539 atmosphere that is associated with evaporation and transpiration of water (i.e. ET). The MOD16 LE
540 and ET are estimated by a modified Penman–Monteith ET method, which uses ground-based
541 meteorological observations and remote sensing data from MODIS (e.g., LAI, albedo, and land
542 cover). Compared with eddy flux measurement, MODIS ET was shown to have a mean absolute
543 error of approximately 0.3 mm day⁻¹ (68). All 8-day composites from 2001 to 2018 were used in this
544 study.

545 ET partition between physical evaporation (E) and transpiration was assessed using the method
546 proposed by Wei et al (2017) (69). This approach presents a ET partitioning algorithm based on
547 the relationships between leaf area index (LAI) and T/(E + T) for different vegetation types. The
548 partition was done as follow:

$$549 \quad \frac{T}{E+T} = 0.66 \times LAI^{0.18} \text{ (croplands)} \quad (4)$$

$$550 \quad \frac{T}{E+T} = 0.69 \times LAI^{0.28} \text{ (pastures)} \quad (5)$$

551 where LAI is the leaf area index, obtained from MOD15A2H collection 6, MODIS LAI product. This
552 is an 8-day composite dataset at 500 m resolution.

553

554 **4.9. Statistical analysis of changes in the climate variables**

555 Temporal changes in rainfall patterns were analyzed using two approaches. First, we analyzed
556 rainfall seasonal patterns in two periods: 1985-2005 representing a period marked by an
557 intensification of forest loss in our study areas, while the percent forest loss in both areas were still
558 below 40%; in the second period between 2005 and 2014, forest loss continued at a lower rate,
559 with the percent forest loss being close to 50%. This assessment was done at monthly time-scale,
560 and considering total rainfall, convective rainfall fraction and stratiform rainfall fraction, separately.
561 Changes in the mean annual rainfall values between these two periods were assessed, and
562 statistical significance was checked using a Welsch t-test. Next, rainfall temporal trends were
563 assessed using a modified version of the Mann-Kendall trend test (70). This modified version of the

564 Mann-Kendall trend test reduces the chances of false positives by accounting for serial correlation,
565 often present in time-series data due to subsequent observations. The magnitude of the trends
566 were assessed using the Sen's slope (71), which is less vulnerable to errors in comparison with
567 least squares estimator of a regression coefficient β , as well as less sensitive to non-normality of
568 the parent distribution and outliers.

569 Changes in EVI, LST, LE and ET associated with forest loss were assessed using a space-for-time
570 substitution approach (SFT) (30, 31). The basic assumption in the SFT is that spatial and temporal
571 variation are equivalent (30). Hence, observations of LST, LE and ET over deforested areas were
572 compared with those obtained over adjacent forests (i.e. intact forests located inside the same $1^\circ \times$
573 1° cell). Deforested areas were identified using the land cover maps. Only areas that were
574 deforested during the entire period of the MODIS time-series used in this study (2001–2018) were
575 used in the analysis. Given the coarser spatial resolution of MODIS data (500 m for LE and ET, ~5
576 km for LST) in comparison with the land cover data (30 m), the influence of pixel mixing on LST,
577 LE and ET retrievals were minimized by eliminating MODIS pixels with more than 10% forest
578 cover. Our analysis did not require re-sampling or pixel aggregation to resize the climate data (i.e.
579 rainfall, LST, ET and LE). Each climatic variable was analyzed independently and, therefore, using
580 the original resolution.

581 The SFT substitution is broadly used to infer temporal changes in ecological and biophysical
582 systems using contemporary spatial patterns (24, 30, 31, 72). This approach is considered an
583 alternative to long-term assessments, particularly in situations when long time-series observations
584 are not available. This is the case of our study, given that the MODIS time-series used in our
585 analysis is available starting from the year 2001.

586

587 **Acknowledgments**

588 This research was funded by the Academy of Finland (decision numbers 318252 and 319905).
589 Temesgen A. Abera thanks SMARTLAND project funded by Academy of Finland (decision number
590 318645). Dr Mika Siljander acknowledges funding from the Ministry for Foreign Affairs of Finland
591 for TAITAGIS project supported by Board of Education of Finland. Luiz E. O. C. Aragão thank
592 FAPESP (grant number 2018/15001-6) and National Council for Scientific and Technological
593 Development (CNPq, grant number 305054/2016-3). Yhasmin M. Moura is funded by the Royal
594 Society under the Newton International Fellowship scheme (grant number NF170036). The authors
595 would like to thank Dr Matheus Nunes for his insightful comments and suggestions in a previous
596 version of this manuscript. The authors also thank two anonymous reviewers for their thoughtful
597 comments and efforts towards improving our manuscript.

598

599

600 References

- 601 1. E. A. Davidson, *et al.*, The Amazon basin in transition. *Nature* **481**, 321–328 (2012).
- 602 2. INPE, PRODES-Monitoramento do Desmatamento da Floresta Amazônica Brasileira por
603 Satélite (2020).
- 604 3. F. J. F. Chagnon, Contemporary climate change in the Amazon. *Geophys. Res. Lett.* **32**,
605 L13703 (2005).
- 606 4. D. V. Spracklen, S. R. Arnold, C. M. Taylor, Observations of increased tropical rainfall
607 preceded by air passage over forests. *Nature* **489**, 282–285 (2012).
- 608 5. D. V. Silvério, *et al.*, Agricultural expansion dominates climate changes in southeastern
609 Amazonia: the overlooked non-GHG forcing. *Environ. Res. Lett.* **10**, 104015 (2015).
- 610 6. E. E. Maeda, *et al.*, Dynamic modeling of forest conversion: Simulation of past and future
611 scenarios of rural activities expansion in the fringes of the Xingu National Park, Brazilian
612 Amazon. *Int. J. Appl. Earth Obs. Geoinf.* **13** (2011).
- 613 7. B. H. Millikan, Tropical Deforestation, Land Degradation, and Society: Lessons from
614 Rondonia, Brazil. *Lat. Am. Perspect.* **19**, 45–72 (1992).
- 615 8. D. S. Alves, Space-time dynamics of deforestation in Brazilian Amazônia. *Int. J. Remote*
616 *Sens.* **23**, 2903–2908 (2002).
- 617 9. A. P. D. Aguiar, G. Câmara, M. I. S. Escada, Spatial statistical analysis of land-use
618 determinants in the Brazilian Amazonia: Exploring intra-regional heterogeneity. *Ecol. Modell.*
619 **209**, 169–188 (2007).
- 620 10. H. P. Binswanger, Brazilian policies that encourage deforestation in the Amazon. *World*
621 *Dev.* **19**, 821–829 (1991).
- 622 11. P. Moutinho, R. Guerra, C. Azevedo-Ramos, Achieving zero deforestation in the Brazilian
623 Amazon: What is missing? *Elem. Sci. Anthr.* **4**, 000125 (2016).
- 624 12. F. J. B. O. de Filho, J. P. Metzger, Thresholds in landscape structure for three common
625 deforestation patterns in the Brazilian Amazon. *Landsc. Ecol.* **21**, 1061–1073 (2006).
- 626 13. A. Mayer, “Agribusiness and Family Farming in Brazil: Competing Modes of Agricultural
627 Production” in *Land Use Competition*, J. Niewöhner, *et al.*, Eds. (Springer International
628 Publishing, 2016), pp. 279–293.
- 629 14. V. Zalles, *et al.*, Near doubling of Brazil’s intensive row crop area since 2000. *Proc. Natl.*
630 *Acad. Sci.* **116**, 428–435 (2019).
- 631 15. D. C. Morton, *et al.*, Cropland expansion changes deforestation dynamics in the southern
632 Brazilian Amazon. *Proc. Natl. Acad. Sci. U. S. A.* **103**, 14637–14641 (2006).
- 633 16. P. G. Curtis, C. M. Slay, N. L. Harris, A. Tyukavina, M. C. Hansen, Classifying drivers of
634 global forest loss. *Science (80-.)*. **361**, 1108–1111 (2018).
- 635 17. J. C. Brown, J. H. Kastens, A. C. Coutinho, D. de C. Victoria, C. R. Bishop, Classifying
636 multiyear agricultural land use data from Mato Grosso using time-series MODIS vegetation
637 index data. *Remote Sens. Environ.* **130**, 39–50 (2013).
- 638 18. G. Oliveira, *et al.*, Effects of land- cover changes on the partitioning of surface energy and

- 639 water fluxes in Amazonia using high- resolution satellite imagery. *Ecohydrology* **12**, e2126
640 (2019).
- 641 19. A. Beltrán-Przekurat, R. A. Pielke Sr, J. L. Eastman, M. B. Coughenour, Modelling the
642 effects of land-use/land-cover changes on the near-surface atmosphere in southern South
643 America. *Int. J. Climatol.* **32**, 1206–1225 (2012).
- 644 20. J. Barlow, *et al.*, The future of hyperdiverse tropical ecosystems. *Nature* **559**, 517–526
645 (2018).
- 646 21. E. T. A. Mitchard, The tropical forest carbon cycle and climate change. *Nature* **559**, 527–534
647 (2018).
- 648 22. N. M. Haddad, *et al.*, Habitat fragmentation and its lasting impact on Earth’s ecosystems.
649 *Sci. Adv.* **1**, e1500052 (2015).
- 650 23. R. Alkama, A. Cescatti, Biophysical climate impacts of recent changes in global forest cover.
651 *Science (80-.)*. **351**, 600–604 (2016).
- 652 24. G. Duveiller, J. Hooker, A. Cescatti, The mark of vegetation change on Earth’s surface
653 energy balance. *Nat. Commun.* **9**, 679 (2018).
- 654 25. T. A. Abera, J. Heiskanen, P. Pellikka, M. Rautiainen, E. E. Maeda, Clarifying the role of
655 radiative mechanisms in the spatio-temporal changes of land surface temperature across
656 the Horn of Africa. *Remote Sens. Environ.* **221**, 210–224 (2019).
- 657 26. J. Wang, *et al.*, Impact of deforestation in the Amazon basin on cloud climatology. *Proc.*
658 *Natl. Acad. Sci.* **106**, 3670–3674 (2009).
- 659 27. J. Khanna, D. Medvigy, S. Fueglistaler, R. Walko, Regional dry-season climate changes due
660 to three decades of Amazonian deforestation. *Nat. Clim. Chang.* **7**, 200–204 (2017).
- 661 28. J. Khanna, D. Medvigy, Strong control of surface roughness variations on the simulated dry
662 season regional atmospheric response to contemporary deforestation in Rondônia, Brazil. *J.*
663 *Geophys. Res. Atmos.* **119**, 13,067–13,078 (2014).
- 664 29. R. Mahmood, R. A. Pielke, C. A. McAlpine, Climate-Relevant Land Use and Land Cover
665 Change Policies. *Bull. Am. Meteorol. Soc.* **97**, 195–202 (2016).
- 666 30. S. T. A. Pickett, “Space-for-Time Substitution as an Alternative to Long-Term Studies” in
667 *Long-Term Studies in Ecology*, G. E. Likens, Ed. (Springer New York, 1989), pp. 110–135.
- 668 31. J. L. Blois, J. W. Williams, M. C. Fitzpatrick, S. T. Jackson, S. Ferrier, Space can substitute
669 for time in predicting climate-change effects on biodiversity. *Proc. Natl. Acad. Sci.* **110**,
670 9374–9379 (2013).
- 671 32. R. A. Pielke, Influence of the spatial distribution of vegetation and soils on the prediction of
672 cumulus Convective rainfall. *Rev. Geophys.* **39**, 151–177 (2001).
- 673 33. D. Ellison, *et al.*, Trees, forests and water: Cool insights for a hot world. *Glob. Environ.*
674 *Chang.* **43**, 51–61 (2017).
- 675 34. D. G. Miralles, P. Gentile, S. I. Seneviratne, A. J. Teuling, Land-atmospheric feedbacks
676 during droughts and heatwaves: state of the science and current challenges. *Ann. N. Y.*
677 *Acad. Sci.* **1436**, 19–35 (2019).
- 678 35. M. J. Lathuillière, M. S. Johnson, S. D. Donner, Water use by terrestrial ecosystems:
679 temporal variability in rainforest and agricultural contributions to evapotranspiration in Mato
680 Grosso, Brazil. *Environ. Res. Lett.* **7**, 024024 (2012).
- 681 36. R. D. V. Epiphanyo, A. R. Formaggio, B. F. T. Rudorff, E. E. Maeda, A. J. B. Luiz, Estimating

- 682 soybean crop areas using spectral-temporal surfaces derived from MODIS images in Mato
683 Grosso, Brazil | Estimativa de áreas de soja usando superfícies espectro-temporais
684 derivadas de imagens MODIS em Mato Grosso, Brasil. *Pesqui. Agropecu. Bras.* **45** (2010).
- 685 37. D. Carrer, G. Pique, M. Ferlicoq, X. Ceamanos, E. Ceschia, What is the potential of
686 cropland albedo management in the fight against global warming? A case study based on
687 the use of cover crops. *Environ. Res. Lett.* **13**, 044030 (2018).
- 688 38. P. J. de O. P. de Souza, E. J. P. da Rocha, A. Ribeiro, E. B. de Souza, Radiation balance in
689 a soybean ecosystem in the Amazon. *Rev. Ciência Agronômica* **41**, 582–592 (2010).
- 690 39. E. E. Maeda, J. Heiskanen, L. E. O. C. Aragão, J. Rinne, Can MODIS EVI monitor
691 ecosystem productivity in the Amazon rainforest? *Geophys. Res. Lett.* **41**, 7176–7183
692 (2014).
- 693 40. A. Huete, *et al.*, Overview of the radiometric and biophysical performance of the MODIS
694 vegetation indices. *Remote Sens. Environ.* **83**, 195–213 (2002).
- 695 41. Y. Li, *et al.*, Local cooling and warming effects of forests based on satellite observations.
696 *Nat. Commun.* **6**, 6603 (2015).
- 697 42. A. Henderson-Sellers, M. F. Wilson, Surface albedo data for climatic modeling. *Rev.*
698 *Geophys.* **21**, 1743 (1983).
- 699 43. A. K. Betts, J. H. Ball, Albedo over the boreal forest. *J. Geophys. Res. Atmos.* **102**, 28901–
700 28909 (1997).
- 701 44. P. K. Panday, M. T. Coe, M. N. Macedo, P. Lefebvre, A. D. de A. Castanho, Deforestation
702 offsets water balance changes due to climate variability in the Xingu River in eastern
703 Amazonia. *J. Hydrol.* **523**, 822–829 (2015).
- 704 45. M. Gloor, *et al.*, Intensification of the Amazon hydrological cycle over the last two decades.
705 *Geophys. Res. Lett.* **40**, 1729–1733 (2013).
- 706 46. K. McGarigal, S. . Cushman, E. Ene, FRAGSTATS v4: Spatial Pattern Analysis Program for
707 Categorical and Continuous Maps (2012).
- 708 47. R. A. Pielke, R. Mahmood, C. McAlpine, Land’s complex role in climate change. *Phys.*
709 *Today* **69**, 40–46 (2016).
- 710 48. J. D. Glover, *et al.*, Increased Food and Ecosystem Security via Perennial Grains. *Science*
711 (80-). **328**, 1638–1639 (2010).
- 712 49. R. Porro, *et al.*, “Agroforestry in the Amazon Region: A Pathway for Balancing Conservation
713 and Development” in *Agroforestry - The Future of Global Land Use*, P. K. R. Nair, D. Garrity,
714 Eds. (Springer Netherlands, 2012), pp. 391–428.
- 715 50. J. D. B. Gil, *et al.*, Tradeoffs in the quest for climate smart agricultural intensification in Mato
716 Grosso, Brazil. *Environ. Res. Lett.* **13**, 064025 (2018).
- 717 51. J. C. dos Reis, *et al.*, Assessing the economic viability of integrated crop–livestock systems
718 in Mato Grosso, Brazil. *Renew. Agric. Food Syst.*, 1–12 (2019).
- 719 52. H. K. Gibbs, *et al.*, Brazil’s Soy Moratorium. *Science (80-).* **347**, 377–378 (2015).
- 720 53. I. Roitman, *et al.*, Rural Environmental Registry: An innovative model for land-use and
721 environmental policies. *Land use policy* **76**, 95–102 (2018).
- 722 54. M. F. Hutchinson, Stochastic space-time weather models from ground-based data. *Agric.*
723 *For. Meteorol.* **73**, 237–264 (1995).
- 724 55. L. McGarigal, B. Marks, “FRAGSTATS Manual: spatial pattern analysis program for

- 725 quantifying landscape structure” (1995).
- 726 56. A. I. Lyapustin, *et al.*, Multi-angle implementation of atmospheric correction for MODIS
727 (MAIAc): 3. Atmospheric correction. *Remote Sens. Environ.* **127**, 385–393 (2012).
- 728 57. G. J. Huffman, *et al.*, The TRMM Multisatellite Precipitation Analysis (TMPA): Quasi-Global,
729 Multiyear, Combined-Sensor Precipitation Estimates at Fine Scales. *J. Hydrometeorol.* **8**,
730 38–55 (2007).
- 731 58. T. Iguchi, T. Kozu, R. Meneghini, J. Awaka, K. Okamoto, Rain-Profiling Algorithm for the
732 TRMM Precipitation Radar. *J. Appl. Meteorol.* **39**, 2038–2052 (2000).
- 733 59. J. Awaka, T. Iguchi, K. Okamoto, TRMM PR Standard Algorithm 2A23 and its Performance
734 on Bright Band Detection. *J. Meteorol. Soc. Japan* **87A**, 31–52 (2009).
- 735 60. M. Steiner, R. A. Houze, S. E. Yuter, Climatological Characterization of Three-Dimensional
736 Storm Structure from Operational Radar and Rain Gauge Data. *J. Appl. Meteorol.* **34**, 1978–
737 2007 (1995).
- 738 61. Z. Wan, New refinements and validation of the collection-6 MODIS land-surface
739 temperature/emissivity product. *Remote Sens. Environ.* **140**, 36–45 (2014).
- 740 62. S.-B. Duan, *et al.*, Radiance-based validation of land surface temperature products derived
741 from Collection 6 MODIS thermal infrared data. *Int. J. Appl. Earth Obs. Geoinf.* **70**, 84–92
742 (2018).
- 743 63. M. Jin, R. E. Dickinson, Land surface skin temperature climatology: benefitting from the
744 strengths of satellite observations. *Environ. Res. Lett.* **5**, 044004 (2010).
- 745 64. E. E. Maeda, P. Hurskainen, Spatiotemporal characterization of land surface temperature in
746 Mount Kilimanjaro using satellite data. *Theor. Appl. Climatol.* **118**, 497–509 (2014).
- 747 65. T. A. Abera, J. Heiskanen, P. Pellikka, E. E. Maeda, Rainfall–vegetation interaction
748 regulates temperature anomalies during extreme dry events in the Horn of Africa. *Glob.*
749 *Planet. Change* **167** (2018).
- 750 66. D. Parastatidis, Z. Mitraka, N. Chrysoulakis, M. Abrams, Online Global Land Surface
751 Temperature Estimation from Landsat. *Remote Sens.* **9**, 1208 (2017).
- 752 67. H. HASHIMOTO, *et al.*, Satellite-based estimation of surface vapor pressure deficits using
753 MODIS land surface temperature data. *Remote Sens. Environ.* **112**, 142–155 (2008).
- 754 68. S. Running, Q. Mu, M. Zhao, A. Moreno, “MODIS global terrestrial evapotranspiration (ET)
755 product 500 m” (2017).
- 756 69. Z. Wei, *et al.*, Revisiting the contribution of transpiration to global terrestrial
757 evapotranspiration. *Geophys. Res. Lett.* **44**, 2792–2801 (2017).
- 758 70. H. B. Mann, Nonparametric Tests Against Trend. *Econometrica* **13**, 245–259 (1945).
- 759 71. P. K. Sen, Estimates of the Regression Coefficient Based on Kendall’s Tau. *J. Am. Stat.*
760 *Assoc.* **63**, 1379–1389 (1968).
- 761 72. T. A. Abera, J. Heiskanen, P. K. E. Pellikka, H. Adhikari, E. E. Maeda, Climatic impacts of
762 bushland to cropland conversion in Eastern Africa. *Sci. Total Environ.* **717**, 137255 (2020).
- 763
- 764